[Supplementary material]

New evidence for Middle Bronze Age chronology from the Syro-Anatolian frontier

Virginia R. Herrmann[1,*], Sturt W. Manning[2,3,4], Kathryn R. Morgan[5], Sebastiano Soldi[1,6] & David Schloen[7]

[1] Institute for Ancient Near Eastern Studies, University of Tübingen, Tübingen, Germany

[2] Cornell Tree Ring Laboratory, Department of Classics, Cornell University, Ithaca, New York, USA

[3] Cornell Institute of Archaeology and Material Studies, Cornell University, Ithaca, New York, USA

[4] The Cyprus Institute, Nicosia, Cyprus

[5] Department of Classical Studies, Duke University, Durham, North Carolina, USA

[6] National Archaeological Museum of Florence, Florence, Italy

[7] Department of Near Eastern Languages and Civilizations, University of Chicago, Chicago, Illinois, USA

[*] Author for correspondence ✉ vrherrmann@gmail.com

OS1: radiocarbon sample descriptions

Further details on the radiocarbon samples from Zincirli Area 2 are provided here (see Table S1 and Figures S1–S3).

Table S1. Results of Radiocarbon Measurements on Samples from Zincirli Area 2.

Lab reference number	Sample	Phase	Context	Material	Date BP	Uncertainty
Tübitak-0461	R18-46.0B#310	Phase 2b*	Fill of drain L17-2118	Free-threshing wheat	3355	26
Tübitak-0474	R18-46.0D#21	Fill for Phase 2b*	Fill of pit L18-2049 into Hilani I socle	Charcoal	2725	25
GrM-13691	R15-679-1a	Phase 4 destruction	Contents of jar C15-452 in Room DD1 (L15-2019)	Bitter vetch	3381	15
GrM-13692	R15-679-1b	Phase 4 destruction	Same as GrM-13691	Bitter vetch	3352	15
GrM-13693	R15-679-2a	Phase 4 destruction	Same as GrM-13691	Bitter vetch	3390	15

GrM-13694	R15-679-2b	Phase 4 destruction	Same as GrM-13691	Bitter vetch	3348	15
GrM-22135	R15-679-2b repeat	Phase 4 destruction	Same as GrM-13691	Bitter vetch	3410	26
OxA-36326	R15-485	Phase 4 destruction	Destruction debris L15-2007 in Room DD2	Olive pit	3828	30
Tübitak-0475	R18-46.0B#23-1	Phase 4 destruction	Contents of vessel C18-46.0B#1 in Room DD11 (L17-2117)	Free-threshing wheat	3392	29
Tübitak-0476	R18-46.0B#23-2	Phase 4 destruction	Same as Tübitak-0475	Free-threshing wheat	3375	26
Tübitak-0477	R18-46.0B#23-3	Phase 4 destruction	Same as Tübitak-0475	Free-threshing wheat	3402	27
Tübitak-0482	R18-46.0B#255-1	Phase 4 destruction	Contents of vessel C18-46.0B#10 in Room DD12 (L18-2079)	Bitter vetch	3335	26
Tübitak-0483	R18-46.0B#255-2	Phase 4 destruction	Same as Tübitak-0482	Bitter vetch	3370	26
Tübitak-0484	R18-46.0B#255-3	Phase 4 destruction	Same as Tübitak-0482	Bitter vetch	3392	26
Tubitak-0462	R18-46.0C#309	Fill for Phase 4	Sounding: fill L18-2082 below Phase 4 street 200 (L18-2008)	Barley seed	3498	28
Tubitak-0480	R18-46.0C#167	Fill for Phase 4	Same as Tübitak-0462	Charcoal	3469	26
Tubitak-0473	R18-46.0C#216	Fill for Phase 4	Sounding: gray ashy layer L18-2083	Charcoal	3476	26
Tubitak-0481	R18-46.0C#245	Fill for Phase 4	Sounding: orange mudbrick detritus L18-2085	Charcoal	3465	26

*Phase 2b was called Phase 3N in Herrmann & Schloen 2021: Table 1.

Figure S1. Radiocarbon samples Tübitak-0482, -0483, and -0484 were on bitter vetch seeds found in situ *in a cooking pot (C18-46.0B#10) in Alcove DD12, Building DD/II. A brick had fallen on this cooking pot, crushing it and sealing its contents. The upper layer of sherds in the photo on the left was removed on the right to reveal its contents of charred bitter vetch seeds. The trench bisecting the context is a modern pipe cut (photographs by H. Brahe; courtesy of the Chicago-Tübingen Excavations at Zincirli).*

Figure S2. Radiocarbon samples Tübitak-0475, -0475, and -0477 were on free-threshing wheat seeds found in a cooking pot (C18-46.0B#1) partially exposed in a baulk (see red arrow), located in Alcove DD11, against the north wall of Building DD/II. The vessel was unambiguously sealed beneath burnt debris from the destruction of Complex DD (as visible in section). More charred grains were found scattered around the installations pictured,

especially the leftmost (L18-2070) (photograph by H. Brahe; courtesy of the Chicago-Tübingen Excavations at Zincirli).

Figure S3. Radiocarbon samples GrM-13691-13694 and GrM-22135 were on bitter vetch seeds found in a smashed storage jar (C15-452) in Room DD1, Building DD/I. Views of the smashed vessel in situ from above (left) and from the side (right) (photographs by L. Stephens; courtesy of the Chicago-Tübingen Excavations at Zincirli).

OS2: radiocarbon analysis and modeling methodology

The organic sample materials from Area 2 were radiocarbon dated at three different laboratories. The samples dated at the Tübitak National 1 MV AMS Laboratory were pretreated and dated according to this laboratory's standard procedures, comprising a modified acid-alkali-acid method, graphisation, and then measurement by AMS with a 1MV NEC Pelletron accelerator (e.g. Marshall *et al*. 2019). The group of samples analyzed at Groningen (GrM) were pretreated and dated following the methods described in Dee et al. (2020). The sample dated at the Oxford Radiocarbon Accelerator Unit was pretreated and dated following methods described previously (Bronk Ramsey *et al*. 2004; Brock *et al*. 2010). The chronological modelling summarized and shown in the main text used OxCal v4.4.4, and we describe this modelling in further detail here. For the archaeological Sequence of four Phases used in the models described below, see the main article text and Table S2 (OxCal Chronological Query Language (CQL2) terms are capitalized in Courier font below (e.g. Sequence, Phase, Boundary)).

Table S2. Summary of the Bayesian models considered for the Zincirli Area 2 radiocarbon sequence.

Model	Description
1a	Initial model based on the stratigraphic sequence of all the samples, with samples from the same closed context combined as weighted averages. An alternative version excluding OxA-36326 is also reported
1b	Same as Model 1a, but with each sample forming an independent age estimate. An alternative version excluding OxA-36326 is also reported
2a	Same as Model 1a, but moving outlier Tübitak-0461 to the MB II destruction Phase and excluding OxA-36326
2b	Same as Model 1b, but moving outlier Tübitak-0461 to the MB II destruction Phase and excluding OxA-36326.
3a	Same as Model 2a, but applying a Levantine radiocarbon offset of 17±4 radiocarbon years for the 19th century BC and 12±5 radiocarbon years for 1700–1500 BC
3b	Same as Model 2b, but applying the same offset as Model 3a

The focus of our chronological modelling was to determine the date of the close of Middle Bronze (MB) II destruction episode. Since we have 11 samples on short-lived plant remains from the fired destruction (excluding OxA-36326 which is likely residual—probably related to earlier EBIV activity attested elsewhere at the site), we may assume that these samples relate closely to this event. A first order approach might be to simply assess a weighted average of all 11 radiocarbon dates on these samples: Figure S4. The data are consistent with potentially representing the same radiocarbon age at the 5% level. The calibrated calendar age suggests a seventeenth century BC date.

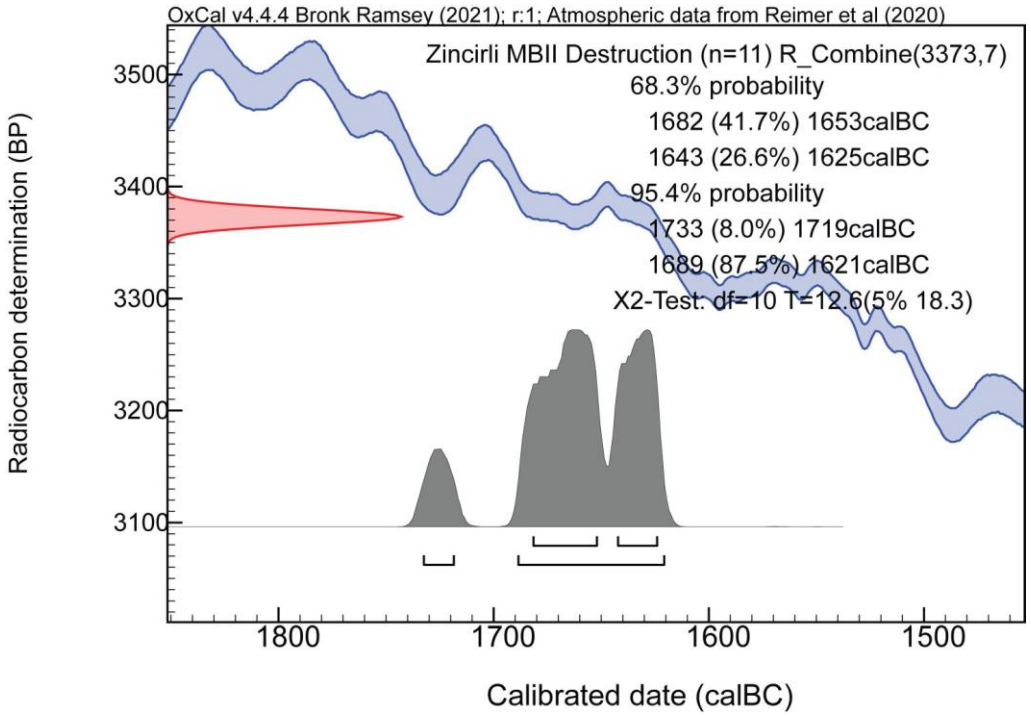

Figure S4. Calibrated calendar age probabilities for the weighted average of the 11 radiocarbon dates on securely associated short-lived plant remains from MBII destruction contexts (Phase 4 Destruction: see Table S1), excluding the likely residual OxA-36326 (calibrated in OxCal (Bronk Ramsey 2009) v4.4.4 using the IntCal20 atmospheric curve (Reimer et al. *2020); figure by S. Manning).*

However, a weighted average is unlikely to offer the most appropriate dating strategy/modelling approach. The dated samples came from three different storage containers and, moreover, there could have been residual or mixed material in any of the containers. The dates may not all reflect the identical original calendar and radiocarbon age. And in any event the destruction was after the date of the samples. In the circumstances of such a widespread fired destruction, we may instead assume that a set of dates on samples comprising stored/in-use short-lived organic materials likely forms an exponential distribution in time, such that most of the samples relate to immediately before (but nonetheless before) the destruction, but some might be a couple to a few years older and a very few might even be older residual material. Thus, we may model the date for the MB II destruction event using a Tau_Boundary paired with a Boundary, such that there is an exponential distribution of the dates within the Phase ramped towards the end of the Phase, with the subsequent Boundary therefore offering the best estimate for the date of the target destruction event. An advantage of this approach is that it allows for the possibility of a small percentage of the samples being,

for some reason, a little older than the final destruction and so does not inflate the date estimated for the destruction event.

The radiocarbon dates on the short-lived samples should provide ages approximately contemporary with their period of growth. We may assume that storage and use occupy no more than a few subsequent years. Despite a long pre-modern history of granaries and other storage technologies in the Mediterranean and Near East (e.g. Privitera 2014; Rosenberg *et al*. 2017; Van Oyen 2020), it is likely that these samples date within a handful of years at most (from growing season and harvest year through storage), and most probably within ~0–2 years, given typical agricultural practices and storage potentials—especially in ceramic vessels as here—and challenges in pre-modern circumstances (e.g. Adamson 1985; Buckland 1990; Panagiotakopulu & Buckland 1991; Halstead 2014: 157–63; Manning 2018: 281–82). Where we have multiple radiocarbon dates on samples of the same material from the same original storage container (three such groups from the Phase 4 destruction: R15-679, R18-46.0B#23 and R18-46.0B#255), we consider two strategies.

First, we combine these same vessel sets together as weighted averages (Ward and Wilson 1978) using the R_Combine command in OxCal. These are Models 1a, 2a and 3a. All pass a Chi-Squared test as consistent with the hypothesis of representing estimates of the same original radiocarbon age value. The SSimple Outlier model is applied to each of the dates in the groups. In the two groups measured at Tübitak (R18-46.0B#23 and R18-46.0B#255), just one individual sample is flagged (and accordingly slightly downweighted) as a possible very minor outlier at ~8% probability (Tübitak-0475 = R18-46.0B#255-1). In contrast, all but one (four of five) of the GrM dates for the R15-679 group are flagged (and accordingly down-weighted) as possible outliers with probabilities of 6% (GrM-13693), 10% (GrM-13692), 10% (GrM-22135) and 16% (GrM-13694). This suggests that the quoted measurement errors are in fact a little too small. After these measurements were run, a study of the Groningen data from their MICADAS AMS (GrM dates) has in fact identified that the measurement errors produced (then) were slightly too small (Aerts-Bijma *et al*. 2021). In the present case, suspicion would fall especially on those four values with quoted measurement errors of just ±15 radiocarbon years. A modest error enlargement would all but resolve the issue: for example, an error multiplier of 1.3 applied to all the GrM dates leaves just one very slight outlier at 7% (GrM-13694). The overall effect is very small. The R15-679 weighted average changes from (no adjustment) 3371±8 to (error multiplier of 1.3 applied to each of the five dates) 3371±10 ^{14}C years BP. We use the laboratory quoted data (Table S1), but note this minor issue.

However, second, we also consider a different and likely more appropriate approach, allowing each date to be an independent estimate. Since the samples comprise multiple separate plant samples (same species) – rather than literally the identical sample material – it is possible for there to be small real variations within each sample, reflecting different plant histories and possibly even the mixing of material from more than one field and/or more than one harvest. The known history and scale of intra-annual and inter-annual variations in atmospheric ^{14}C (e.g. Levin *et al*. 2010; Reimer *et al*. 2020) mean that some variation in results might be expected and hence treating the set as a whole might be a more appropriate route to modelling the Boundary for the end of Phase 4 Destruction event using a Tau_Boundary paired with a Boundary. These are Models 1b, 2b and 3b. The exception could be the pair of measurements on the exact same sample preparation material (GrM-13694 and GrM-22135). However, as the very different GrM numbers indicate, these samples were run at substantially different times, and so we choose to regard the two data as different and include them both separately in the 'b' models.

A problem with the 'a' approach is that the population of data (three weighted averages) is really too small to allow a proper exponential Phase modelling. The end result is that there is a lack of definition to the end (recent side) of the Destruction Boundary, since there is no other proximate subsequent constraint. Thus, in each of Models 1a, 2a and 3a there is a long tail to the Destruction Boundary (Figure S5). This is clearly a problem in Model 3a, where the additional factor of growing season/curve adjustment is allowed for. In contrast, the 'b' models provide a sufficient population of data in the exponential Phase so that the subsequent Boundary, defining the Destruction episode, is much better defined. For this reason, we prefer and recommend use of the 'b' model results.

In addition to the radiocarbon dates from the Phase 4 destruction, we have dates from stratigraphically-defined contexts before and after the destruction: the archaeological Sequence of four Phases is explained in the main article text. Each model uses this Sequence. Models 1a and 1b employ all the data as listed in Table S1 given the two different approaches just described (we also consider the Phase 4 destruction Boundary from Models 1a and 1b runs excluding OxA-36326: see Figure S5). Models 2a, 2b, 3a and 3b apply minor changes each described below. We test for outliers within the models, and downweight them in the analysis, for the dates on the short-lived samples, or for the weighted averages from short-lived samples, using the OxCal General Outlier model (Bronk Ramsey 2009b). The SSimple Outlier model is applied to the dates within a weighted average. There are also a few dates on wood charcoal samples. We have no information on whether these were outermost tree-rings.

Thus, these samples likely include issues of in-built age. We apply the OxCal Charcoal Outlier model to allow approximately for such likely in-built age (thus shifting the modelled ages towards more recent possible ages) (Bronk Ramsey 2009b).

Model 1a applies the above Sequence and criteria to the data in Table S1 with weighted averages on the samples of the same material from the same container: see Figure 7. The results from Model 1a for the Phase 4 destruction Boundary with, and excluding, OxA-36326 are shown in Figure S5. Model 1b treats each of the Phase 4 destruction dates as separate estimates: Figure 8. Again, results from Model 1b for the Phase 4 destruction Boundary with, and excluding, OxA-36326 are shown in Figure S5. Runs of Model 1a and 1b highlight two observations. First, as noted already, it is evident that the OxA-36326 sample is much older than the other samples from the MBII destruction and is likely residual: its age would suggest that it probably derives from EBIV activity—plausible since EBIV activity is attested elsewhere at the site. The second obvious observation: the non-modelled calibrated calendar age range for Tübitak-0461 is 1737–1540 (95.4%), and so it is clearly an MB II date and not Iron Age, and thus is a residual sample as placed in its Iron Age find context. Hence, both models identify this sample as a likely outlier, and fail to find a plausible Iron Age date for this sample. We could either exclude this date or place it in the Phase with the Phase 4 MB II destruction samples (where it clearly derives from, originally). Since there is no intervening evidence of occupation between the MBII destruction and the Iron Age, this re-attribution seems reasonable (and it is entirely possible that MBII destruction debris filtered into the Iron Age drain that cut it). Hence, we keep Tübitak-0461 as valid/useful evidence, but move it to the Phase 4 MBII destruction (in Models 2a, 3a, 2b and 3b).

Two other key issues identified in recent work are relevant to Levantine radiocarbon chronology. These are, first, small regional radiocarbon offsets related to different plant growing seasons comparing those of a range of plants from the lower elevation and warmer regions of the Levant with the trees comprising the IntCal20 record, and, second, indications that some regions of the calibration curve that comprise mainly legacy conventional, versus recent AMS ^{14}C, data may need modest but (at high resolution) important revision (Dee *et al*. 2010; Manning *et al*. 2018, 2020a, 2020b; Pearson *et al*. 2020; Reimer *et al*. 2020; Wacker *et al*. 2020). Originally, when comparisons were made between new AMS ^{14}C data on Egyptian-Levantine samples and the *then* current radiocarbon calibration curves (IntCal04, or IntCal13), comprised in these periods primarily of conventional radiocarbon data (e.g., gas proportional counting or liquid scintillation technologies), it seemed that average offsets of around 19±5 radiocarbon years existed (Dee *et al*. 2010; Bronk Ramsey *et al*. 2010; Manning

et al. 2018). However, where the IntCal20 calibration curve is substantially informed by numerous recent AMS radiocarbon data (thus the second millennium AD, and 1700–1500 BC), then these differences typically reduce, on average, to somewhere around 12±5 radiocarbon years (Manning *et al*. 2020a, 2020b; see also Brehm *et al*. 2021, who observe that the Levantine ^{14}C offsets identified against the previous IntCal13 calibration dataset are reduced, but importantly still present, versus the recent ETH dataset). This latter difference likely represents the expression of growing season differences recording different portions of the annual atmospheric radiocarbon cycle, having removed what appears to be an additional conventional versus AMS ^{14}C offset in some cases. This growing season offset likely applies for Levantine cases where the plants concerned have spring-summer harvest periods (e.g. most field crops) earlier than the main growing seasons of the trees from central and northern Europe and North America providing the majority of the IntCal20 record in this period. However, it probably does not apply to cases where the relevant growing season runs through the summer: e.g., to radiocarbon dates on olive seeds.

Does such a Levantine radiocarbon offset apply at Zincirli in the Northern Levant? The agricultural field areas proximate to the site are at moderate elevation, >480m, the winter sees average overnight temperatures <10°C December to March, and the site is in a relatively well-watered area (average precipitation in the region >600mm) (taking for example the İslahiye meteorological record, within 10km, as indicative). The site falls into the southeastern Anatolian region (Unal *et al*. 2003). Thus the traditional growing season for field crops is in fact likely more similar to the typical growing season in Central Europe, mainly spring and into summer with a summer harvest, rather than the earlier schedule observed in warmer and more arid and lower elevation areas of the Eastern Mediterranean/Near East—such as in much of the Southern Levant. Therefore, the observed radiocarbon offset, linked to differences in growing seasons, observed in the Southern Levant and Egypt or for some trees in the southern central Anatolian region, is likely less pronounced for Zincirli. The IntCal20 record therefore likely offers a reasonable guide. Nonetheless, in Models 3a and 3b, revising Models 2a and 2b, we allow for a putative Levantine offset assuming this represents a maximum case (and since the effect is to slightly lower calendar ages this represents the minimum age model for the MBII destruction). Analysis of radiocarbon data from Kültepe, Acemhöyük and Karahöyük, after correction for a likely problem with IntCal20 around a wiggle in the nineteenth century BC, found an approximately 17±4 radiocarbon year error on average for an MBA tree-ring series versus IntCal20 (Manning *et al*. 2020b; the offset without excluding the problematic wiggle was

approximately 22±5 radiocarbon years). This was in a period where IntCal20 comprises legacy conventional radiocarbon data. In contrast, as noted above, during periods where IntCal20 is largely informed by modern AMS radiocarbon data, such offsets are smaller, e.g., 12±5 radiocarbon years for the Southern Levant and Egypt. These values are likely over-estimations for the Zincirli context, as noted above. Thus, as a 'worst case' in Models 3a and 3b, we apply a 17±4 radiocarbon years offset for the data lying on the legacy portions of IntCal and a 12±5 radiocarbon years offset for the data likely lying in the AMS-dominated period of IntCal 1700–1500 BC. This should yield the latest plausible date estimate for the Zincirli MBII destruction. We note that the 'a' approach (Models 1a, 2a, 3a), where there are just three (weighted average) data in the exponential Phase defining the subsequent Boundary and destruction event (effectively too small a population really for this type of model), exhibits the effects of this limitation in the Model 3a case. Although, as in all Models, dating probability centers in the later seventeenth century BC (e.g., the most likely 45% of probability lies between *c*. 1638–1600 BC), there is, however, a very long tail. For this reason, we prefer the 'b' models where the model allows the data to better describe the expected circumstances.

Figure 9a overlays and compares each of the eight probability distributions for the Phase 4 MBII destruction from Figure S5. The combined probability from all eight model runs places the single overall most likely range with approximately 73.2% of the total probability *c*. 1662–1606 BC. When we then combine just the preferred Model 1b (excluding OxA-36326 as residual), Model 2b and Model 3b, the single most likely highest probability region, with approximately 56.2% of total probability, lies 1632–1610 BC (Figure 9b). We employ this range, merging the various assumptions and variables, as our preferred best dating estimate. The model results shown in Figures 7–9 and Figure S5 and listed in Table 1 in the main text come from runs of each model with kIterations set at 3000 and are selected as typical examples from a set of several such runs. There are small variations in modelled results between runs of such models and especially in those areas where there are less data or few constraints. The OxCal runfile for Model 1b is provided below in Table S3 as an example.

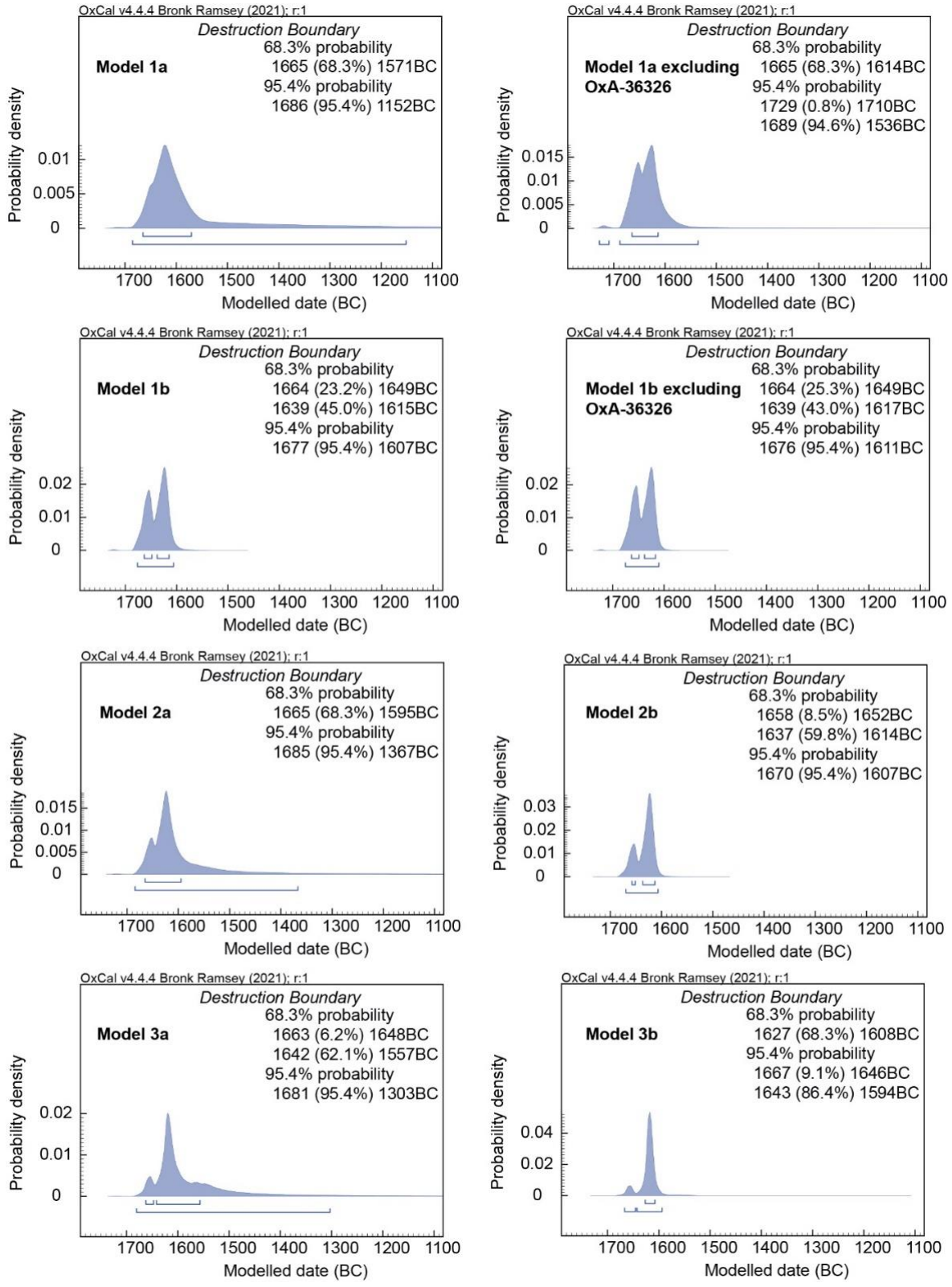

Figure S5. Modelled calendar age probabilities from all models (Models 1a and 1b including and excluding outlier OxA-36236) for the Boundary 'Destruction' that defines the end of Phase 4 and so forms the date estimate for the Zincirli Area 2, Phase 4 MB II destruction event (prepared by S. Manning).

Table S3. Model 1b OxCal runfile as an example.

```
Options()
 {
  Resolution=1;
 };
 Plot("Zincirli Area 2 MBII Destruction")
 {
  Outlier_Model("Charcoal",Exp(1,-10,0),U(0,3),"t");
  Outlier_Model("General",T(5),U(0,4),"t");
  Sequence ()
  {
   Boundary("Start MBI-II evidence")
   {
    color="Green";
   };
   Phase("Fill for Ph.4, TPQ for MBII Area 2, MBI-II")
   {
    R_Date("Tubitak-0480 R18-46.0C#167 charcoal",3469,26)
    {
     Outlier("Charcoal",1);
    };
    R_Date("Tubitak-0473 R18-46.0C#216 charcoal",3476,26)
    {
     Outlier("Charcoal",1);
    };
    R_Date("Tubitak-0481 R18-46.0C#245 charcoal",3465,26)
    {
     Outlier("Charcoal",1);
    };
    R_Date("Tubitak-0462 R18-46.0C#309 barley seeds",3498,28)
    {
     Outlier("General",0.05);
    };
```

```
 Interval("Interval MBI-II");
 Date("Date Estimate MBI-II and TPQ for MBII")
 {
  Color="blue";
 };
};
Boundary ("End MBI-II")
{
 color="Green";
};
Interval("Period end MBI-II to start MBII");
Boundary ("Start MBII")
{
 color="Green";
};
Phase("MBII before destruction")
{
 Date("Date MBII Period, early to later");
 Interval("Interval MBII pre-destruction");
};
Sequence()
{
 Tau_Boundary("T")
 {
  color="Green";
 };
 Phase("MBII Destruction Area 2 Ph.4")
 {
  Label("Apparent Residual Date from MBII context: likely really EBIV matching EBIV elsewhere at site");
  R_Date("OxA-36326 R15-485 3828 Area 2 Ph 4 destruction olive pit",3828,30)
  {
   Outlier("General", 0.05);
  };
```

```
R_Date("GrM-13691 R15-679 bag 1",3381,15)
{
 Outlier("General",0.05);
};
R_Date("GrM-13692 R15-679 bag 1-B",3352,15)
{
 Outlier("General",0.05);
};
R_Date("GrM-13693 R15-679 bag 2",3390,15)
{
 Outlier ("General",0.05);
};
R_Date("GrM-13694 R15-679 bag 2-B",3348,15)
{
 Outlier ("General",0.05);
};
R_Date("GrM-22135 R15-679 bag 2-B repeat",3410,26)
{
 Outlier ("General",0.05);
};
R_Date("Tubitak-0475 R18-46.0B#23-1",3392,29)
{
 Outlier ("General",0.05);
};
R_Date("Tubitak-0476 R18-46.0B#23-2",3375,26)
{
 Outlier ("General",0.05);
};
R_Date("Tubitak-0477 R18-46.0B#23-3",3402,27)
{
 Outlier ("General",0.05);
};
R_Date("Tubitak-0482 R18-46.0B#255-1",3335,26)
{
```

```
  Outlier ("General",0.05);
 };
 R_Date("Tubitak-0483 R18-46.0B#255-2",3370,26)
 {
  Outlier ("General",0.05);
 };
 R_Date("Tubitak-0484 R18-46.0B#255-3",3392,26)
 {
  Outlier ("General",0.05);
 };
};
Boundary("Destruction")
{
 color="Blue";
};
};
Boundary("Start TAQ Iron Age")
{
 color="Green";
};
Phase("Phase 2b")
{
 R_Date("Tubitak-0474 R18-46.0D#21 charcoal",2725,25)
 {
  Outlier("Charcoal", 1);
 };
 R_Date("Tubitak-0461 R18-46.0B#310 wheat",3355,26)
 {
  Outlier("General",0.05);
 };
 //Clearly residual in IA context likely from the Phase 4 MBA destruction
};
Boundary("End Sequence")
{
```

```
  color="Green";
 };
};
Difference("MBII","Destruction","Start MBII");
};
```

OS2: Detailed description and sources for Figure 10

We present here more detailed information about Figure 10 with an explanation of the symbology and the sources of information employed.

Figure 10. This is an interpretative figure showing radiocarbon dates and archaeological phasing of north Levantine sites destroyed in the late/final MB II and dendrochronological dates from Kültepe, correlated with historical events and compared with five proposed absolute chronologies for those events. HC = High Chronology; hMC = High-Middle Chronology; lMC = Low-Middle Chronology; LC = Low Chronology; NC/ULC = New Chronology/Ultra-Low Chronology (Pruzsinszky 2009; Höflmayer & Manning 2022). The green gradient indicates the apparent best fit with the majority of the dates reported. For each site, the archaeological phases are placed in approximate correlation to the historical events above. Date ranges from reported radiocarbon analyses or statements are given below relevant phases with the following symbology employed:

(1) quotation marks: radiocarbon results reported in a publication without giving the raw dates;

(2) bold: summaries of multiple dates that are part of a modelled sequence (68.3% highest posterior density reported);

(3) green: results of radiocarbon-wiggle-matching of tree-ring sequences;

(4) italics: dates on wood charcoal (where the sample type is not reported, it is assumed to be on charcoal);

(5) regular type: single dates on short-lived samples;

(6) dates connected to a circle give a *terminus post quem* or *ad quem* for a phase's construction;

(7) dates connected to a diamond come from the phase's destruction.

All published single dates have been (re)calibrated with OxCal (Bronk Ramsey 2009a) v.4.4.4 software using the IntCal20 curve (Reimer et al. 2020) except where source radiocarbon data was unavailable (see (1) above); the 68.3% highest posterior density range (or the largest sub-range where there is a single large sub-range indicated) is reported here.

Sources: Kültepe (Manning *et al*. 2020b: 4); Zincirli (this article); Tilmen (Marchetti 2008: 467, n. 12, 2010: 370, n.6); Kinet (Novák *et al*. 2017: 181); Tell Atchana (Yener 2021: 580, fig. 8); Oylum (Engin 2020: 284); Tell Mardikh (Fiorentino *et al*. 2008: tab. 2, fig. 3); Umm el-Marra (Schwartz 2017: 99, tab. 5.5); Lidar (Görsdorf *et al.* 2002: 65); Zeytinli Bahçe (Balossi *et al*. 2007: 375).

References

ADAMSON, P.B. 1985. Problems over storing food in the ancient Near East. *Die Welt des Orients* 16: 5–15.

AERTS-BIJMA, A. *et al*. 2021. An independent assessment of uncertainty for radiocarbon analysis with the new generation high-yield accelerator mass spectrometers. *Radiocarbon* 63: 1–22. https://doi.org/10.1017/RDC.2020.101

BALOSSI, F., G.-M. DI NOCERA & M. FRANGIPANE. 2007. The contribution of a small site to the study of settlement changes on the Turkish Middle Euphrates between the third and second millennium B.C.: preliminary stratigraphic data from Zeytinli Bahçe Höyük (Urfa), in C. Kuzucuoğlu & C. Marro (ed.) Sociétés humaines et changement climatique à la fin du Troisième Millénaire: une crise a-t-elle eu lieu en Haute Mésopotamie? Actes du Colloque de Lyon, 5-8 décembre 2005: 355–81. Paris: De Boccar.

BREHM, N. *et al.* 2021. Eleven-year solar cycles over the last millennium revealed by radiocarbon in tree rings. *Nature Geoscience* 14: 10–15. https://doi.org/10.1038/s41561-020-00674-0

BROCK F., T.F.G. HIGHAM, P. DITCHFIELD & C. BRONK RAMSEY. 2010. Current pretreatment methods for AMS radiocarbon dating at the Oxford Radiocarbon Accelerator Unit (ORAU). *Radiocarbon* 52: 103–12. https://doi.org/10.1017/S0033822200045069

BRONK RAMSEY C. 2009a. Bayesian analysis of radiocarbon dates. Radiocarbon 51: 337–60. https://doi.org/10.1017/S0033822200033865

BRONK RAMSEY, C. 2009b. Dealing with outliers and offsets in radiocarbon dating. *Radiocarbon* 51: 1023–45. https://doi.org/10.1017/S0033822200034093

BRONK RAMSEY C., T. HIGHAM & P. LEACH. 2004. Towards high-precision AMS: progress and limitations. *Radiocarbon* 46: 17–24. https://doi.org/10.1017/S0033822200039308

BRONK RAMSEY, C. *et al.* 2010. Radiocarbon-based chronology for dynastic Egypt. *Science* 328: 1554–57. https://doi.org/10.1126/science.1189395

BUCKLAND, P.C. 1990. Granaries stores and insects: the archaeology of insect synanthropy, in D. Fournier & F. Sigaut (ed.) *La Préparation Alimentaire des Céreals*: 69–81. Rixensart: PACT.

DEE, M.W. *et al.* 2010. Investigating the likelihood of a reservoir offset in the radiocarbon record for ancient Egypt. *Journal of Archaeological Science* 37: 687–93. https://doi.org/10.1016/j.jas.2009.09.003

– 2020. Radiocarbon dating at Groningen: new and updated chemical pretreatment procedures. *Radiocarbon* 62: 63–74. https://doi.org/10.1017/RDC.2019.101

ENGIN, A. 2020. Oylum and Alalakh: cultural relations in the second millennium BC, in K. A. Yener & T. Ingman (ed.) Alalakh and its neighbours: proceedings of the 15th anniversary symposium at the New Hatay Archaeology Museum, 10–12 June 2015 (Ancient Near Eastern Studies Supplement 55): 275–305. Leuven: Peeters.

FIORENTINO, G. *et al*. 2008. Third millennium BC climate change in Syria highlighted by carbon stable isotope analysis of ^{14}C-AMS dated plant remains from Ebla. *Palaeogeography, Palaeoclimatology, Palaeoecology* 266: 51–58. https://doi.org/10.1016/j.palaeo.2008.03.034

GÖRSDORF, J., H. HAUPTMANN, & G. KASCHAU. 2002. ^{14}C-Datierungen zur Schichtabfolge des Lidar Höyük, Südost-Türkei. Berliner Beiträge zur Archäometrie 19: 63–70.

HALSTEAD, P. 2014. *Two oxen ahead: pre-mechanized farming in the Mediterranean*. Chichester: Wiley Blackwell. https://doi.org/10.1002/9781118819333

HERRMANN, V.R. & J.D. SCHLOEN. 2021. Middle Bronze Age Zincirli: the date of 'Hilani I' and the end of MB II. Bulletin of the American Schools of Oriental Research 385: 33–51. https://doi.org/10.1086/711911

LEVIN, I. *et al*. 2010. Observations and modelling of the global distribution and long-term trend of atmospheric $^{14}CO_2$. *Tellus B* 62: 26–46. https://doi.org/10.1111/j.1600-0889.2009.00446.x

MANNING, S.W. 2018. Some perspectives on the frequency of significant, historically forcing drought and subsistence crises in Anatolia and region, in E. Holt (ed.) *Water and power in past societies* (IEMA Proceedings, volume 7): 279–95. Albany: State University of New York Press.

MANNING, S.W. *et al*. 2018. Fluctuating radiocarbon offsets observed in the southern Levant and implications for archaeological chronology debates. *Proceedings of the National Academy of Sciences of the USA* 115: 6141–46. https://doi.org/10.1073/pnas.1719420115

– 2020a. Mediterranean radiocarbon offsets and calendar dates for prehistory. *Science Advances* 6: eaaz1096. https://doi.org/10.1126/sciadv.aaz1096

– 2020b. Radiocarbon offsets and Old World chronology as relevant to Mesopotamia, Egypt, Anatolia and Thera (Santorini). *Scientific Reports* 10: 137835. https://doi.org/10.1038/s41598-020-69287-2

MARCHETTI, N. 2008. A preliminary report on the 2005 and 2006 excavations at Tilmen Höyük, in J.M. Cordoba *et al*. (ed.) *Proceedings of the 5th international congress on the archaeology of the Ancient Near East, Madrid, April 3–8 2006*: 465–79. Madrid: Consejo superior de investigaciones cientificas.

– 2010. A preliminary report on the 2007 and 2008 excavations and restorations at Tilmen Höyük, in P. Matthiae, F. Pinnock, L. Nigro & N. Marchetti (ed.) Proceedings of the 6th international congress on the archaeology of the Ancient Near East, May 5th–10th 2008, "Sapienza"-Università di Roma: 369–83. Wiesbaden: Harrassowitz.

MARSHALL, P. *et al*. 2019. ^{14}C wiggle-matching of short tree-ring sequences from post-medieval buildings in England. *Nuclear Instruments and Methods in Physics Research Section B: Beam Interactions with Materials and Atoms* 438: 218–26. https://doi.org/10.1016/j.nimb.2018.03.018

NOVÁK, M. *et al*. 2017. A comparative stratigraphy of Cilicia. *Altorientalische Forschungen* 44: 150–86. https://doi.org/10.1515/aofo-2017-0013

PANAGIOTAKOPULU, E. & P.C. BUCKLAND. 1991. Insect pests of stored products from Late Bronze Age Santorini, Greece. *Journal Stored Products Research* 27: 179–84. https://doi.org/10.1016/0022-474X(91)90043-C

PEARSON, C. *et al.* 2020. Annual variation in atmospheric ^{14}C between 1700 BC and 1480 BC. *Radiocarbon* 62: 939–52. https://doi.org/10.1017/RDC.2020.14

PRIVITERA, S. 2014. Long-term grain storage and political economy in Bronze Age Crete: contextualizing Ayia Triada's silo complexes. *American Journal of Archaeology* 118: 429–49. https://doi.org/10.3764/aja.118.3.0429

REIMER, P.J. *et al.* 2020. The IntCal20 Northern Hemisphere radiocarbon age calibration curve (0–55 kcal BP). *Radiocarbon* 62: 725–57. https://doi.org/10.1017/RDC.2020.41

ROSENBERG, D., Y. GARFINKEL & F. KLIMSCHA. 2017. Large-scale storage and storage symbolism in the ancient Near East: a clay silo model from Tel Tsaf. *Antiquity* 91: 885–900. https://doi.org/10.15184/aqy.2017.75

SCHWARTZ, G.M. 2017. Western Syria and the third- to second-millennium B.C. transition, in F. Höflmayer (ed.) *The late third millennium in the ancient Near East: chronology, C14, and climate change* (Oriental Institute Seminars 11): 87–128. Chicago (IL): Oriental Institute.

UNAL, Y., T. KINDAP & M. KARACA. 2003. Redefining the climate zones of Turkey using cluster analysis. *International Journal of Climatology* 23: 1045–55. https://doi.org/10.1002/joc.910

VAN OYEN, A. 2020. *The socio-economics of Roman storage: agriculture, trade, and family*. New York: Cambridge University Press. https://doi.org/10.1017/9781108850216

WACKER, L. *et al*. 2020. Findings from an in-depth annual tree-ring radiocarbon intercomparison. *Radiocarbon* 62: 873–82. https://doi.org/10.1017/RDC.2020.49

WARD, G.K. & S.R. WILSON. 1978. Procedures for comparing and combining radiocarbon age determinations: a critique. *Archaeometry* 20: 19–31. https://doi.org/10.1111/j.1475-4754.1978.tb00208.x

YENER, K.A. 2021. Some thoughts about Middle Bronze Age Alalakh and Ugarit: reassessing an Alalakh wall painting with archival data, in V. Matoian (ed.) *Ougarit, un anniversaire. Bilans et recherches en cours* (Ras Shamra-Ougarit 28): 573–88. Leuven: Peeters.